Available online at www.sciencedirect.com
ScienceDirect
Earth and Planetary Science Letters 259 (2007) 360–371
EPSL
www.elsevier.com/locate/epsl

Magnetite (U–Th)/He dating and its application to the geochronology of intermediate to mafic volcanic rocks

Terrence J. Blackburn *, Daniel F. Stockli, J. Douglas Walker

University of Kansas Department of Geology, 1475 Jayhawk Blvd, Lindley Hall 120, Lawrence, KS 66044, USA

Received 21 November 2006; received in revised form 29 April 2007; accepted 30 April 2007
Available online 8 May 2007
Editor: R.W. Carlson

Abstract

We present a new approach to dating intermediate to mafic volcanic rocks using magnetite (U–Th)/He geochronology. Magnetite is common in volcanic rocks that typically do not contain easily datable minerals such as sanidine or zircon. Analytical procedures for producing magnetite (U–Th)/He ages have been developed, including mineral separation, sample air-abrasion to correct for α-ejection effects, He extraction/measurement, sample dissolution, and anion-exchange column chemistry procedures. Dated magnetite crystals were non-skeletal, euhedral to subhedral, and 100–300 μm in size. To test the reliability of this new geochronometer, four basaltic to andesitic samples lacking sanidine or zircon were dated by both magnetite (U–Th)/He and whole-rock $^{40}Ar/^{39}Ar$ methods. For two samples, the ages from the different geochronometers are in excellent agreement (<1%). A third sample with a poorly behaved $^{40}Ar/^{39}Ar$ age spectrum affected by ^{39}Ar recoil yielded a well-defined magnetite (U–Th)/He age that is consistent with $^{40}Ar/^{39}Ar$ age data from similar nearby volcanic rocks. The final sample, however, exhibited a near 40% discrepancy between the two methods, despite yielding reproducible magnetite (U–Th)/He ages. In all cases, the multi-aliquot magnetite (U–Th)/He ages ($n>7$) exhibit 3–11% (2σ) variation about the mean age, indicating that reproducibility for magnetite (U–Th)/He ages is comparable to that of apatite and zircon (U–Th)/He analyses. In order to assess the He retentivity, we conducted a single magnetite helium diffusion experiment, yielding a well-behaved Arrhenius relationship and a closure temperature of ~250 °C ($dT/dt=10$ °C/myr). Magnetite's high He retentivity coupled with (U–Th)/He age reproducibility demonstrates good potential for magnetite (U–Th)/He dating as an alternative volcanic geochronometer, particularly in cases where samples yield inconclusive or uninterpretable $^{40}Ar/^{39}Ar$ ages.
© 2007 Elsevier B.V. All rights reserved.

Keywords: (U–Th)/He; magnetite; helium; thermocrhonology; geochronology; volcanic

1. Introduction

Mafic to intermediate extrusive rocks are the most common volcanic rock types on the earth's surface, dominating the upper oceanic crust as well as many tectonically active portions of the continental crust. Reliable geochronology of these rocks is critical for resolving a wide range of geologic problems, including paleomagnetic time-scale calibrations, chronostratigraphic constraints on evolutionary and paleoclimatic history, as well as tectonic timing and rate studies. Despite their widespread occurrence and importance in unraveling temporal aspects of earth processes, precise dating of mafic to intermediate volcanic rocks is often hindered by the aphanitic nature of these rocks and the

* Corresponding author.
E-mail address: terrence@mit.edu (T.J. Blackburn).

0012-821X/$ - see front matter © 2007 Elsevier B.V. All rights reserved.
doi:10.1016/j.epsl.2007.04.044

absence of commonly dated phases. The most commonly employed technique for constraining the eruption ages of such rocks has been ground-mass or whole-rock K–Ar or $^{40}Ar/^{39}Ar$ geochronology. However, analytical and geological complications, such as ^{39}Ar recoil or excess ^{40}Ar can result in poorly-behaved and difficult to interpret age data when using these techniques. The ability to reliably date aphantic mafic to intermediate volcanic rocks requires geochronologists to resolve these problems and/or develop alternative geochronologic methods.

In this study, we present results from (U–Th)/He dating of magnetite that demonstrate the potential the technique has as an alternative method to dating mafic to intermediate composition volcanic rocks. Magnetite is found in nearly all types of extrusive rocks and is common in intermediate to mafic volcanic rock types that typically do not contain minerals such as sanidine, zircon, and biotite. (U–Th)/He dating of apatite and zircon from quickly cooled volcanic standard samples has been carried out extensively to monitor laboratory procedures (House et al., 2000; Reiners and Farley, 1999; Farley et al., 2002; Min et al., 2006; Aciego et al., 2003; Blackburn et al., 2005; Stockli et al., 2005). Several studies have built on these efforts and have explicitly employed (U–Th)/He geochronometry to time the cooling of xeno- and phenocrystic minerals in volcanic rocks, thus demonstrating that the (U–Th)/He system can provide reliable age constraints on a wide range of minerals and volcanic rocks to constrain eruption ages (Min et al., 2006; Aciego et al., 2003; Blackburn et al., 2005; Stockli et al., 2005; Blondes et al., 2007; Schmitt et al., 2006) . We developed analytical procedures to date magnetite by the (U–Th)/He method, including mineral separation, sample abrasion, ^{4}He extraction/measurement, sample dissolution, and anion-exchange column chemistry protocols. To test the reliability of this geochronometer, four magnetite bearing basaltic to andesitic volcanic rocks from the western Basin and Range Province, United States were dated by magnetite (U–Th)/He geochronometry.

2. Analytical techniques

2.1. Sample characterization and mineral separation

For this study, only euhedral to subhedral magnetite grains or equidimensional magnetite fragments were selected for (U–Th)/He analysis, avoiding composite grains showing complex intergrowth of magnetite with other mineral phases or aphantic groundmass. Samples for this study were selected after careful characterization of magnetite size and texture using standard thin section and backscattered electron (BSE) imaging techniques. Analyzing equigranular magnetite grains as opposed to skeletal or vein-like magnetite growth is an important distinction to be made to avoid complications related to α-implantation or ejection effects (Haggerty, 1991). A photomicrograph of sample 12-7-01C shows three representative euhedral magnetite grains with no skeletal intergrowth (Fig. 1A). Detailed BSE imaging of magnetite crystals from the same sample shows similar euhedral habits, corroborating the lack of complex intergrowth, and reveals a non-spongy internal grain texture with few mineral inclusions and no obvious exsolution textures (Fig. 1B).

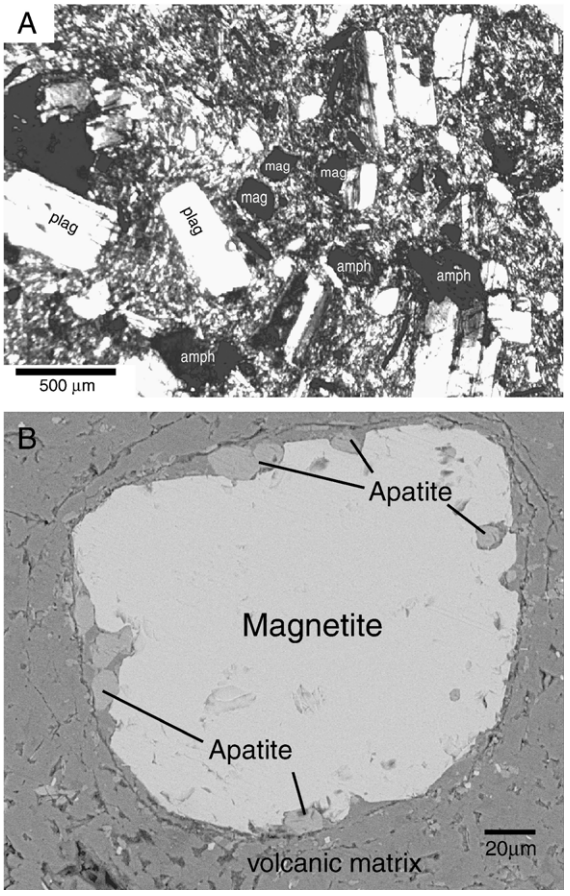

Fig. 1. (A). Photomicrograph of three magnetite grains in a standard thin section from sample 12-7-01C. These large magnetite grains are representative of magnetite grains dated by (U–Th)/He methods. Fig 1 (B) Back Scatter Electron imaging of a magnetite grain from sample 12-7-01C. BSE imaging supports interpretation that grains are non-composite, non-skeletal, and euhedral to anhedral in shape. Small apatite grains concentrate along the edges. Mechanical abrasion of magnetite grains removes the outer 20–30 µm affected by alpha implantation from these apatite grains and surrounding matrix.

Mineral separation for geochronological studies is an often overlooked and underappreciated effort. Isolation of many minerals requires time-consuming, multi-step mineral separation procedures (e.g., zircon and feldspar). Magnetite, however, because of its high magnetic susceptibility can be easily isolated from most rocks. In this study, samples were crushed using standard jaw crusher and disc mill techniques and subsequently cleaned and density sorted using a water table. Magnetite was then manually extracted from the heavy mineral separate using a magnet and sieved into different size fractions (>500, 250, 125 μm). Magnetite crystals from the 250–500 μm size fraction were carefully screened and hand selected according to several criteria, including habit, alteration, and morphology. This final hand selection can be tedious due to the magnetic properties of magnetite, requiring that magnetite separates are spread on double-sided tape and selected using plastic tweezers.

2.2. Air abrasion and α-implantation/ejection correction

It is well documented that during decay of U and Th, alpha (α) particles are emitted with high kinetic energy and travel significant distances before coming to rest. This decay energy is taken up mostly in the form of energetic emission of the α-particle and α-recoil of the parent nucleus (Meesters et al., 2002; Farley et al., 1996; Farley, 2002). This presents a complication for the He dating method in that α-particles may be ejected out of the crystal being dated or injected into the crystal from decay occurring in surrounding grains. For mineral phases with considerable U and Th content, this loss is commonly corrected for by using the measured surface to volume ratio of a crystal and α-stopping distances to solve for the fraction (F_T) of retained α-particles (Farley et al., 1996; Ziegler, 1977). More recently an alternative technique has utilized mechanical air abrasion to remove α-ejection effected outer portions of mineral grains (Min et al., 2006), following procedures similar to those developed by Krogh (Krogh, 1982). If both parent nuclides and ^{4}He daughter are homogenously distributed throughout the dated crystal, mechanical abrasion should offer a reliable and improved approach to obtaining high quality (U–Th)/He geochronometric data from quickly cooled volcanic rocks (Min et al., 2006). A homogenous distribution of radiogenic ^{4}He requires that no diffusive loss has occurred as a result of slow cooling or reheating of the sample. The presence of U- and Th-bearing inclusions, zoning, or skeletal magnetite growth would all violate fundamental assumptions, resulting in heterogeneous distributions of U and Th (and thus ^{4}He).

More important for the application of magnetite (U–Th)/He dating is the fact that magnetite is commonly characterized by U and Th concentrations lower than the surrounding mineral phases and/or aphantic matrix. Long stopping distances of alpha particles during decay of U and Th are likely to result in considerable alpha implantation (Verchovsky and Begemann, 1993; Spencer et al., 2004). Therefore, in the case of magnetite, mechanical air abrasion is primarily employed to remove the outer portions of mineral grains affected by α-implantation from the matrix and U- and Th-bearing neighboring mineral phases.

In each of the rocks dated in this study, the U and Th concentrations of the dated magnetite are significantly lower than those of the surrounding matrix. While whole rock concentrations in the four samples range from 8–14 ppm U and 1–4 ppm Th, magnetite concentrations for these same rocks contain as little as 100–1000 ppb U and 300–1000 ppb Th. This difference in parent nuclide concentration will result in He implantation into the magnetite grain margins. Therefore, mechanical abrasion used by Min and others (Min et al., 2006) to remove marginal He depletion, in this case actually corrects magnetite (U–Th)/He ages for α-implantation from the parent nuclide enriched host rock matrix.

BSE imaging of a polished thin section of sample 12-7-01C shows magnetite in its proper textural context and reveals another complication alleviated by mechanical abrasion. The magnetite is commonly found in contact with small (~10 μm) apatite crystals (Fig. 1B). The close spatial relationship between these mineral phases suggests that the magnetite grain will experience significant α-particle implantation from the (presumably) U- and Th-bearing apatite. Mechanical abrasion of the outer portion of magnetite grains will not only abrade away these surficial apatite grains but also abrade and remove any magnetite that been enriched in ^{4}He daughter by implantation from the apatite.

All magnetite grains dated in this study were abraded in pyrite for 6–8 h, removing at least the outer ~30 μm of each grain or about twice the average alpha stopping distance in magnetite (~16 μm). Magnetite grain size and shape were monitored during the abrasion process by periodically halting the abrasion process, photographing and measuring grain size. The 6–8 h abrasion time employed in this study was intentionally overly cautious, ensuring time for sufficient (>20 μm) removal of material from all portions of the grain including pointed terminations. After abrasion, the once euhedral magnetite grains should be near spherical in shape.

2.3. Laser He extraction and measurement

Depending on grain size and U and Th concentrations 2–10 abraded magnetite grains were loaded into platinum tubes and weighed to determine the total mass of magnetite. Samples with low U and Th concentrations ($\ll$1 ppm) require up to 1.5 mg of magnetite to ensure daughter and parent nuclide sample amounts are well above instrumental detection limits for both noble gas and ICP-MS analyses. Magnetite samples wrapped in platinum tubes were heated by a Nd:YAG laser to ~1300 °C for 10 min (Tagami et al., 2003). While most magnetite grains readily degassed, some samples required multiple laser He extractions to ensure total He extraction (<1%), a behavior commonly exhibited by high retentive phases such as zircon. After laser degassing and cryogenic purification, ^{4}He concentrations were measured by isotope dilution using a ^{3}He tracer. Sample ^{4}He amounts were calibrated against a manometrically-determined ^{4}He standard, analyzed multiple times daily to correct for instrument drift.

2.4. Sample dissolution and column chemistry

For U, Th, and Sm concentration determinations, the magnetite samples were removed from the platinum tubes, spiked with an HNO_3-based ^{230}Th–^{235}U–^{149}Sm tracer, and dissolved using a 5:1 mixture of concentrated HF and 7 N HNO_3 at ~150 °C. This solution was dried down and dissolved in concentrated HCl at ~150 °C to ensure conversion of insoluble ThF_4 complexes, dried down again, and redissolved in ~60 μl of 7N HNO_3 for ion exchange column chemistry. Relatively large magnetite samples (up to 1.5 mg) result in high concentrations of major elements (e.g., Fe, Ti, Mg) that tend to degrade the quality of U, Th, and Sm measurements by ICP-MS (Baker et al., 2002; Tsuyoshi et al., 2003). Therefore, all dissolved magnetite samples were purified using a two-step anion exchange column procedure to (1) separate U and Th from major elements and REE (Table 1A) and (2) separate Sm (+REE) from major elements (Fe, Ti) (Table 1B). Separating U–Th–Sm from major elements using anion-exchange resin column chemistry yields significantly better and more reproducible U–Th–Sm ICP-MS data (Baker et al., 2002; Tsuyoshi et al., 2003) All U–Th–Sm amounts were determined by ICP-MS isotope dilution using a mixed spike which was calibrated against a gravimetric 1 ppb U–Th–Sm standard solution. U–Th–Sm analyses for samples 12-7-01C, 1003-CF-02, VH38-02 were conducted using a VG P54 MC-ICP-MS at the Department of Terrestrial Magnetism at the Carnegie Institute. Sample 12-4-01A was analyzed using a VG PQII quadrupole ICP-MS at the Isotope Geochemistry Laboratories at the University of Kansas.

Table 1
Summary of proecdures for the separation of U, Th and Sm

(A) U–Th micro column chemistry	Reagent	Vol (μl)
Resin	AG1×8 resin	100
Clean	H_20	200
Clean	6 N HCL	200
Clean	H_20	100
Condition	7 N HNO_3	150
Load sample (Collect Sm)	7 N HNO_3	60
Wash (Collect Sm)	7 N HNO_3	350
Collect U–Th	6 N HCL	250
Collect U–Th	H_20	250
(B) Sm column chemistry	**Reagent**	**Vol (ml)**
Resin	AG50W×8 resin	2
Clean	6 N HCL	20
Clean	H_20	5
Condition	2.5 N HCL	20
Load sample	2.5 N HCL	0.5
Wash (Elute Majors)	2.5 N HCL	12
Collect Sm	6 N HCL	10

3. Results

3.1. Magnetite helium diffusion experiment

To quantitatively interpret magnetite (U–Th)/He ages, it is important to understand helium retentivity and diffusion kinetics of magnetite as a function of temperature. We therefore conducted a helium diffusion experiment using a light-bulb heating apparatus (Farley et al., 1999) at temperatures between 350–620 °C with an temperature accuracy of±3 °C and step stability of <1 °C. This fractional-loss step-heating experiment, utilizing procedures outlined in Fechtig and Kalbitzer (Fechtig and Kalbitzer, 1966), was conducted on sieved, ~500 μm diameter magnetite fragments collected from a kimberlitic magnetite vein from Bala, Kansas. The magnetite diffusion experiment consists of ~50 steps (0.3–12 h in duration) that yield a well-behaved Arrhenius relationship excellent linear correlations (R^2=0.98) that is characterized by a minor decrease in diffusivity during the cycled heating schedule. The diffusion experiment yields an activation energy (E_a) and a log frequency factor (log D_0/a^2) of 220+9/−13 kJ/mol and 6.8 +0.7/−0.5, respectively (Fig. 2). These values allow for the calculation of a closure temperature (T_c) of 248 °C, assuming a spherical geometry of

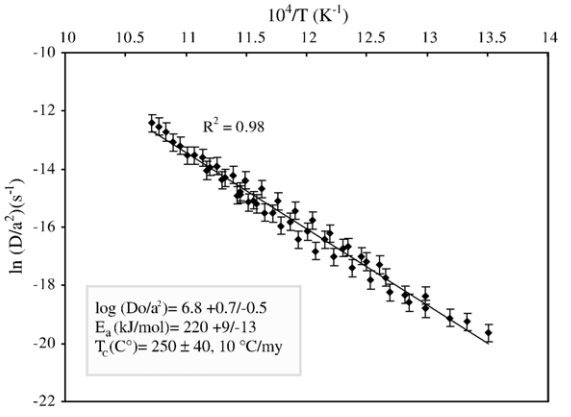

Fig. 2. Plot of data from magnetite step heating diffusion experiment. Data defines linear Arrhenius relationship indicating volume diffusion behavior for helium in magnetite. Error bars on individual heating steps are directly from instrumental temperature accuracy of ±3 °C. Activation energy (E_a) and log frequency factor of (Log D_0/a^2) derived from this line are of 220+9/−13 kJ/mol and a 6.8+0.7/−0.5 respectively and are used to calculate a closure temperature (T_C) of 248 °C (cooling rate=10 °C/myr). Errors calculated from york regression through the line. All errors are 2σ. See data repository for complete data from this experiment.

diffusion and a cooling rage of 10 °C/Myr (Dodson, 1972). See Table 1 in the Appendix for complete data from this experiment.

3.2. Magnetite (U–Th)/He geochronology

Four samples from the western United States were selected from middle Miocene to Pliocene suites of andesitic to basaltic rocks and dated by magnetite (U–Th)/He methods. Two samples (12-7-01C, 12-4-01A) are from middle Miocene rocks in the northern Slate Range, California; the other two samples (1003-CF-02, VH38-02) are from the eastern Queen Valley area, Nevada (Tincher and Stockli, 2004). The final age uncertainty (2σ) for each individual aliquot is propagated from the analytical errors on each measurement used to calculate the (U–Th–[Sm])/He date (U, Th, Sm, He). A mean error-weighted age, uncertainty, and MSWD are calculated using Isoplot (Ludwig, 2004) for each set of multi-aliquot magnetite (U–Th)/He analyses. In all but one case (12-4-01A), the final age uncertainty is smaller than the dispersion of ages about the mean (MSWD ≫ 1). Over-dispersion of (U–Th)/He ages is a commonly observed phenomenon that is typically attributed to heterogeneous distributions of parent nuclides (Min et al., 2006; Boyce and Hodges, 2005). In the case of magnetite (U–Th)/He ages, apatite (or other inclusions), and extremely low U and Th concentrations are the likely contributors to over-dispersed age data. Despite this, the 2σ variability about the mean age for these magnetite (U–Th)/He dates (3–11%) is comparable to that of apatite (~6%) and zircon (~8%) (U–Th)/He analyses. Fig. 3 and Table 2 summarize the magnetite (U–Th)/He data.

3.3. $^{40}Ar/^{39}Ar$ whole-rock geochronology data

Samples used in study for magnetite (U–Th)/He geochronology were also dated using groundmass step-heating $^{40}Ar/^{39}Ar$ methods. Samples from the Slate Range, California (12-7-01C and 12-4-01A) were dated at the Massachusetts Institute of Technology $^{40}Ar/^{39}Ar$ facility, while samples collected from Queen Valley, Nevada (VH-38-02, 1003-CF-02) were dated by $^{40}Ar/^{39}Ar$ methods at the New Mexico Geochronological Research laboratory (NMGRL) (Heizler and Sanders, 2005). All $^{40}Ar/^{39}Ar$ analyses except for sample 1003-CF-02 yield reasonably well-behaved release spectra with well-defined plateau ages. Except where specified, we define plateau ages as consisting of three contiguous heating steps within error of each other and total >50% of the cumulative ^{39}Ar released (Fleck et al., 1977). $^{40}Ar/^{39}Ar$ results are presented below together with the (U–Th[–Sm])/He age data. All $^{40}Ar/^{39}Ar$ age data is summarized in Fig. 4 and Table 3. See Table 2 in the Appendix for complete data set.

3.4. Magnetite (U–Th)/He and $^{40}Ar/^{39}Ar$ age data from case studies

3.4.1. Sample 12-4-01A

Magnetite (U–Th)/He analyses from sample 12-4-01A give a weighted mean age of 12.8±0.5 Ma with a MSWD=1.13 (Fig. 3A; Table 2). Each aliquot was relatively small (200–350 μg) due to relatively high parent nuclide concentrations of ~0.25 ppm U and ~1 ppm Th. Sm concentrations range from 3 to 5 ppm, affecting the calculated (U–Th[–Sm])/He age up to 5%. Sample bulk U and Th concentrations are 3.5 ppm and 13.7 ppm, respectively. Groundmass $^{40}Ar/^{39}Ar$ analysis of sample 12-4-01A shows a well-behaved plateau age composed of three contiguous heating steps accounting for near 70% of the ^{39}Ar released (Fig. 4A). The calculated age from this plateau is 12.8±0.4 Ma (Fig. 4A), while the normal and inverse isochron ages are 13.3±0.5 Ma and 13.3±0.5 Ma, respectively. These $^{40}Ar/^{39}Ar$ ages are in excellent agreement with the magnetite (U–Th)/He age of 12.8±0.5 Ma (Fig. 3A).

3.4.2. Sample 12-7-01C

(U–Th)/He analyses of ten multi-grain magnetite aliquots yield a mean age of 10.4±0.3 Ma (Fig. 3B and

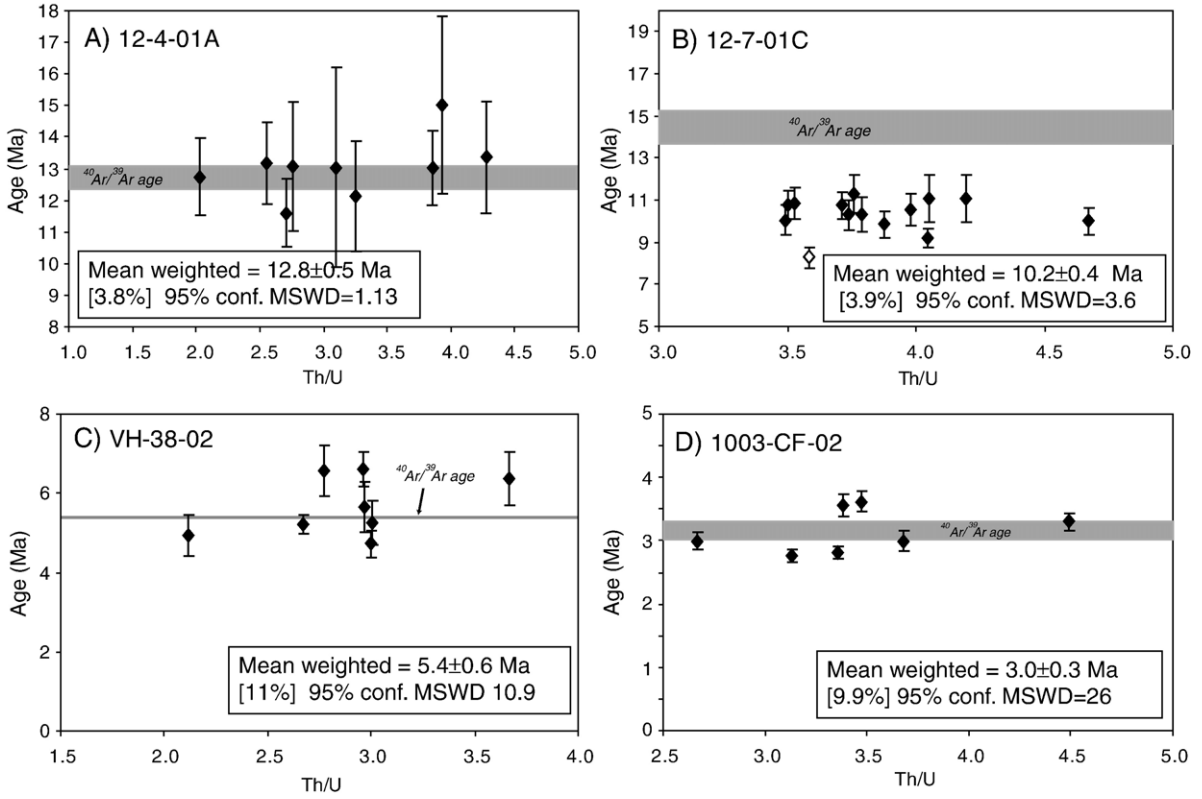

Fig. 3. Summary diagrams for magnetite (U–Th)/He data plotted against Th/U. Error bars for each data point are propagated from individual analytical errors of He, U, Th, and Sm. The sample age and uncertainty is the mean error-weighted age, calculated using Isoplot (Ludwig, 2004). Clustering of aliquot ages in terms of Th/U suggests that analyzed magnetite grains are free of U- and Th-bearing secondary phases (inclusions). For comparison, the data is projected on top of the $^{40}Ar/^{39}Ar$ age error envelope (gray) for the corresponding sample (see Table 3 and Fig. 4 for $^{40}Ar/^{39}Ar$ interpretations).

Table 2). Each aliquot consisted of 5–10 air-abraded magnetite crystals. Magnetite from this basaltic andesite sample is characterized by relatively high parent nuclide concentrations (~0.5 ppm U, 1–2 ppm Th), allowing for relatively small sample sizes (~150–250 μg).. Significant Sm concentrations in magnetite aliquots from sample 12-7-01C range from ~4–10 ppm affecting the (U–Th[–Sm])/He ages by about 10% (Table 2). SEM back-scattered electron imaging of magnetite in polished thin sections showed the presence of small apatite inclusions (~5–10 μm diameter) potentially explaining the slightly higher U, Th, and Sm concentrations compared to the other magnetite analyzed in this study. The imaging also revealed larger apatite (~15 μm diameter) adjacent to magnetite, illustrating the need for air abrasion to eliminate the potential effect of He implantation from neighboring apatite (Fig. 1B). Sample bulk U and Th concentrations are 3.8 ppm and 14.2 ppm, respectively.

Sample 12-7-01C yields a well-behaved $^{40}Ar/^{39}Ar$ plateau age with four contiguous steps totaling near 80% of released ^{39}Ar (Fig. 4B). The calculated age from this plateau is 14.5±0.9 Ma (MSWD=0.13). Both the normal and inverse isochron ages are in good agreement with the plateau age, yielding ages of 14.7±0.7 Ma and 14.5±1.0 Ma, respectively (Table 3). Both the plateau and isochron ages do not agree with the 10.4±0.3 Ma age determined by the magnetite (U–Th)/He method (Fig. 3B).

3.4.3. Sample VH-38-02

Magnetite from sample VH38-02 is characterized by the lowest U, Th, and Sm concentrations of any samples in this study, with average concentrations as low as ~100 ppb U and ~300 ppb Th. Thus, this sample required analysis of ~1 mg aliquots of magnetite (split between several sub-aliquots in separate platinum jackets during laser heating) to ensure sufficient parent nuclides for measurement by ICP-MS (Table 2). After ^{4}He measurement and removal from the platinum jackets, sub-aliquots were combined for U–Th–Sm analysis, with each combined sample aliquot ranging in

Table 2
Magnetite (U–Th)/He age data

Sample	Age (Ma)	± (Ma)	U (ppm)	Th (ppm)	Sm (ppm)	Th/U	He (ncc/mg)	mass (mg)
12-4-01A, Slate Range, CA, lat, long: 35.8836, −117.2574								
12-4-01A-7	13.0	3.2	0.313	0.968	5.479	3.09	0.93	0.18
12-4-01A-8	13.4	1.8	0.384	1.640	8.136	4.28	1.36	0.27
12-4-01A-9	15.0	2.8	0.342	1.345	7.756	3.93	1.32	0.20
12-4-01A-10	13.1	2.0	0.348	0.959	4.333	2.76	0.97	0.27
12-4-01A-11,12	13.2	1.3	0.347	0.885	3.829	2.55	0.94	0.50
12-4-01A-13, 15	11.6	1.1	0.371	1.004	5.521	2.71	0.92	0.61
12-4-01A-16,17	13.0	1.2	0.317	1.226	5.630	3.86	1.03	0.69
12-4-01A-18,19	12.7	1.2	0.317	0.642	3.702	2.02	0.77	0.64
12-4-01A-22	12.1	1.7	0.212	0.689	3.011	3.26	0.59	0.46
Mean error weighted=12.8±0.5 [3.8%] 95% conf, MSWD=1.13								
12-7-01C, Slate Range, CA, lat, long: 35.9640, −117.3247								
12-7-01C-11	9.9	0.7	0.52	2.00	8.40	3.88	1.26	0.22
12-7-01C-12*	8.3	0.5	0.71	2.54	9.38	3.59	1.39	0.18
12-7-01C-13	9.2	0.4	0.50	2.01	5.68	4.05	1.14	0.17
12-7-01C-14	10.3	0.7	0.49	1.82	7.53	3.74	1.22	0.17
12-7-01C-15	11.3	0.9	0.41	1.55	7.92	3.76	1.16	0.20
12-7-01C-16	10.3	0.8	0.55	2.09	10.81	3.79	1.43	0.16
12-7-01C-17	10.8	0.6	0.35	1.31	4.95	3.71	0.92	0.21
12-7-01C-18	10.6	0.7	0.45	1.77	7.94	3.98	1.19	0.23
12-7-01C-19	10.0	0.7	0.46	1.61	7.82	3.49	1.11	0.15
12-7-01C-20	10.0	0.6	0.41	1.91	6.84	4.67	1.11	0.28
12-7-01C-21	10.8	0.7	0.27	0.96	3.92	3.50	0.70	0.25
12-7-01C-22	10.8	0.7	0.54	1.92	8.78	3.53	1.41	0.21
12-7-01C-24	11.1	1.1	0.37	1.51	5.74	4.05	1.04	0.24
12-7-01C-25	11.1	1.1	0.44	1.83	8.25	4.20	1.25	0.32
Mean error weighted=10.2±0.4 [3.9%] 95% conf, MSWD=3.6								
VH-38-02 Basalt, NV, lat, long: 37.98422, −175.7983								
VH3802Mag-1	6.6	0.6	0.112	0.309	1.788	2.77	0.16	0.45
VH3802Mag-2	6.4	0.7	0.112	0.411	2.091	3.66	0.17	0.64
VH3802Mag-3	5.6	0.6	0.101	0.299	1.336	2.97	0.12	0.48
VH3802Mag-4	5.3	0.5	0.107	0.322	1.718	3.01	0.13	0.86
VH3802Mag-5	4.9	0.5	0.150	0.317	1.233	2.12	0.14	0.69
VH3802Mag-6	5.2	0.2	0.076	0.203	0.616	2.67	0.08	0.80
VH3802Mag-7	4.7	0.3	0.081	0.242	0.983	3.00	0.08	0.54
VH3802Mag-8	6.6	0.4	0.082	0.244	1.137	2.96	0.12	0.60
Mean error weighted=5.4±0.6 [11%] 95% conf, MSWD=10.9								
1003-CF-02, Basalt, NV, lat, long: 37.9983, −175.7392								
1003CF01MAG-1	3.3	0.1	0.191	0.859	2.032	4.49	0.17	0.48
1003CF01MAG-3	3.6	0.2	0.219	0.759	2.256	3.47	0.18	0.86
1003CF01MAG-4	2.8	0.1	0.296	0.927	2.277	3.13	0.18	0.69
1003CF01MAG-5	2.8	0.1	0.249	0.836	1.992	3.36	0.16	0.80
1003CF01MAG-6	3.0	0.2	0.225	0.827	2.661	3.68	0.16	0.54
1003CF01MAG-7	3.6	0.2	0.163	0.552	1.746	3.38	0.13	0.60
1003CF01MAG-8	3.0	0.1	0.233	0.623	2.106	2.67	0.14	0.69
Mean error weighted=3.0±0.3 [9.9%] 95% conf, MSWD=26								

* Rejected.

weight from ~500–600 μg, translating to 50–60 pg of uranium (~100 ppb U). Despite this analytical challenge, seven aliquots, each consisting of approximately ten grains (grain size >100 ìm) yield a mean magnetite (U–Th)/He age of 5.6±0.6 Ma (Fig. 3C). Samarium concentrations ranged from 1–1.5 ppm affecting the (U–Th[–Sm])/He age by ~10%. Sample bulk U and Th concentrations are 1.9 ppm and 8.7 ppm, respectively.

Sample VH-38-02 yields a complicated $^{40}Ar/^{39}Ar$ release spectrum with younger and older apparent ages

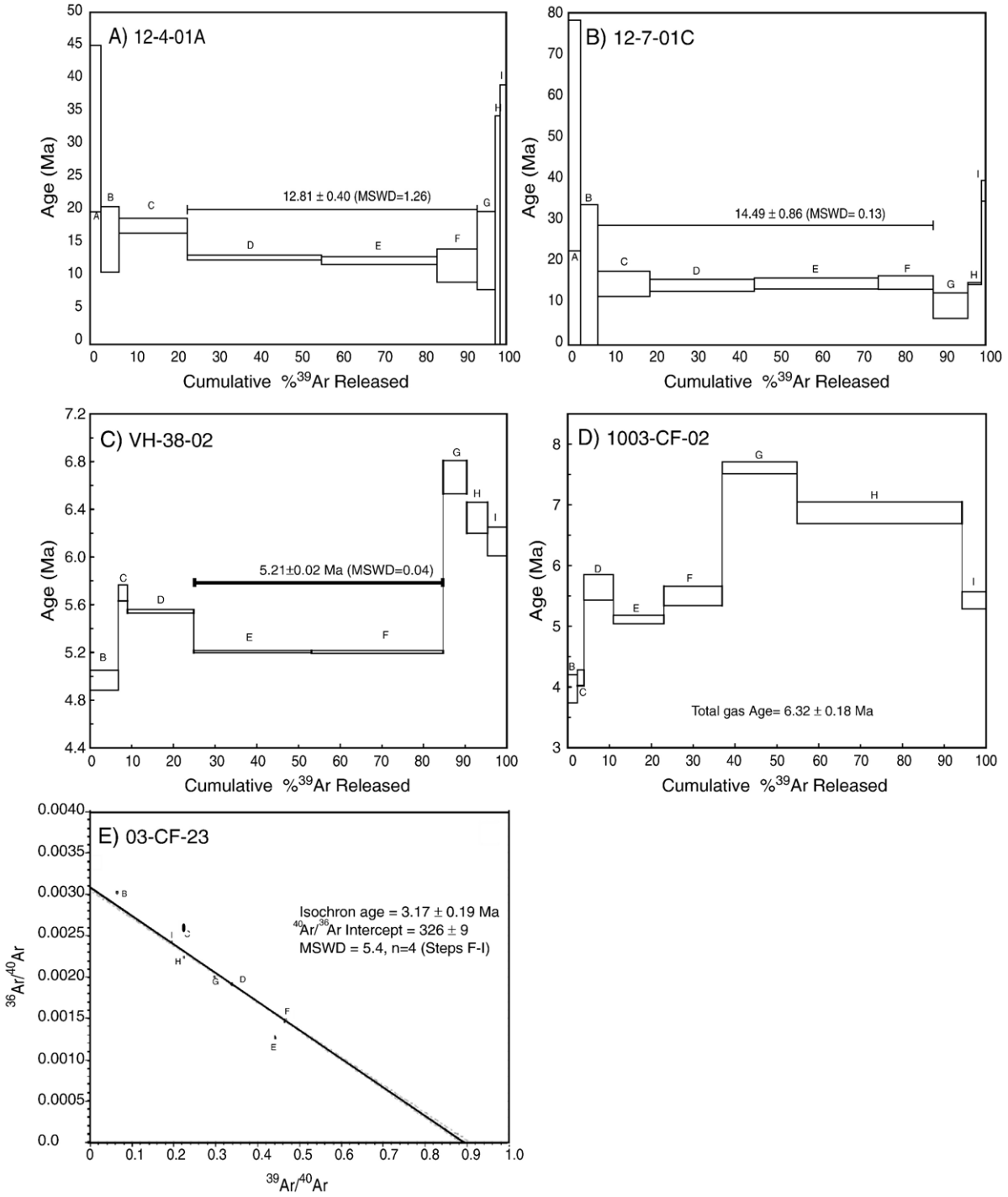

Fig. 4. $^{40}Ar/^{39}Ar$ step-heating experiments on volcanic groundmass samples. All $^{40}Ar/^{39}Ar$ analyses, except for sample 1003-CF-02, yield reasonably well-behaved release spectra with well-defined plateau ages.

during initial heating steps and older ages during high temperature steps (Fig. 4C). These changes in age are not correlated with variations in radiogenic yield or K/Ca values. Two contiguous heating steps (E and F) define a pseudo-plateau (not three contiguous heating steps as required by Fleck (Fleck et al., 1977), representing the bulk of gas (~60% ^{39}Ar released), and yield an age of 5.21±0.02 Ma (MSWD=0.04)

Table 3
Summary of results from $^{40}Ar/^{39}Ar$ step-heating experiments

				Age (Ma)	±2 sigma
12-4-01A, Slate Range, CA, lat, long: 35.8836, −117.2574					
Total gas age	–	$n=9$	–	14.08	0.77
Plateau	Steps D–F	$n=3$	MSWD=1.26	12.81	0.4
Inv Isochron	Steps D–F	$n=3$	MSWD=0.66	13.27	0.51
12-7-01C, Slate Range, CA, lat, long: 35.9640, −117.3247					
Total gas age	–	$n=9$	–	14.97	1.44
Plateau	Steps C–F	$n=4$	MSWD=0.13	14.49	0.86
Inv Isochron	Steps C–F	$n=4$	MSWD=0.2	14.51	0.97
VH-38-02 Basalt, NV, lat, long: 37.98422, −175.7983					
Total gas age	–	$n=8$	–	5.436	0.033
Plateau	Steps E–F	$n=2$	MSWD=0.04	5.21	0.02
1003-CF-02, Basalt, NV, lat, long: 37.9983, −175.7392					
Total gas age	–	$n=8$	–	6.32	0.18
03-CF-23 Basalt, NV, lat, long: 37.98939, −175.8066					
Total gas age	–	$n=8$	–	3.78	0.06
Inv Isochron	Steps F–I	$n=4$	MSWD=5.4	3.17	0.19

(Fig. 4C). Considerable data scatter related to the anomalous high- and low-temperature release steps do not allow for the calculation of reliable normal isochron and inverse isochron ages (Heizler and Sanders, 2005). This $^{40}Ar/^{39}Ar$ age is within error of the 5.6±0.6 Ma of the magnetite (U–Th)/He age (Fig. 3C).

3.4.4. Sample 1003-CF-02

Nine air-abraded magnetite aliquots yield a weighted mean magnetite (U–Th)/He age for this sample of 3.1± 0.3 Ma (Fig. 3D). Each aliquot consisted of at least ten large grains (>200 μm) divided between several platinum jackets for ^{4}He laser extraction and measurement. Uranium concentrations for this sample range from 100–200 ppb and 500–900 ppb of Th. Samarium concentrations ranged from 2–3 ppm lowering the calculated (U–Th[–Sm])/He age by ~5%. Sample bulk U and Th concentrations are 1.6 ppm and 8.1 ppm, respectively.

Sample 1003-CF-02 yields an uninterpretable $^{40}Ar/^{39}Ar$ age spectrum characterized by non-contiguous steps that define a hump-shaped age spectrum with younger apparent ages during both low-temperature initial and high-temperature final heating steps (Fig. 4D). The total gas age for sample is 6.3±0.2 Ma, but the irreproducible steps suggest that this age has little meaning. A different sample from a nearby volcanic unit of the same eruptive interval (sample 03-CF-23) yields an inverse isochron age of 3.2±0.2 Ma (Fig. 4E) which is in excellent agreement with the 3.1±0.3 Ma magnetite (U–Th)/He age for sample 1003-CF-02. Sample 03CF23 is not from the same exact flow unit as magnetite from sample 1003-CF-02, but chemical and stratigraphic correlations suggest that the two samples belong to different flows of the same eruptive interval (Bradley, 2004).It is reasonable to use the $^{40}Ar/^{39}Ar$ from 03CF323 to evaluate the accuracy of magnetite (U–Th)/He data from sample 1003CF02.

4. Discussion

4.1. Magnetite helium diffusion and retentivity

A single magnetite diffusion experiment (~50 heating steps) conducted on sieved fragments from a kimberlitic magnetite vein from NE Kansas shows that He diffusion in magnetite is dominated by thermally activated volume diffusion. The experimental data exhibit an Arrhenius relationship that is used to derive an activation energy (E_a) of 220+9/−13 kJ/mol and a log D_0/a^2 value of 6.8+0.7/−0.5 (Fig. 2). These kinetic He diffusion parameters translate to a nominal closure temperature (T_c) for He in magnetite of ~248 °C, assuming a cooling rate of 10 °C/Myr (Dodson, 1972). There is considerable structure in the magnetite He diffusion Arrhenius plot, showing a slight decrease in diffusivity during the cycled heating schedule. The dispersion in data is likely attributable to surface-related artifacts and/or variability in grain size due to imperfect sorting of effective grain radii during sample sieving. While the average diameter of magnetite used in the diffusion experiment was ~500 μm, slightly smaller or fractured grains are expected to be less retentive during the diffusion experiment. It should be noted that the diffusion experiment was carried out on fragments (~500 μm) larger than the magnetite grains (~200–300 μm) dated in this case study. Therefore dated, abraded magnetite grains are expected to be slightly less retentive, but no systematic data quantifying the influence of grain size on magnetite He retentivity exist. The nominal He closure temperature for magnetite is significantly higher than that for zircon and titanite (U–Th)/He, but lower than traditional $^{40}Ar/^{39}Ar$ geochronometers (e.g., biotite). The T_c for the $^{40}Ar/^{39}Ar$ method applied to groundmass samples of mafic to intermediate compositions is difficult to evaluate since its diffusion characteristics are compositionally and mineralogically controlled by the dominant K-bearing phases. While it is difficult to evaluate how susceptible $^{40}Ar/^{39}Ar$ groundmass and plagioclase ages are to

thermal resetting, the new magnetite helium diffusion data allow us to estimate and model temperatures required to perturb the magnetite (U–Th)/He radiometric clock (e.g., in response to a younger overlying basalt flow). In summary, the He retentivity suggests that magnetite quantitatively retains helium over geologic time and represents a viable geochronometer for the determination of eruption ages of mafic and intermediate volcanic rocks.

4.2. Magnetite (U–Th)/He geochronological results

New magnetite (U–Th)/He ages were obtained from middle Miocene to Pliocene basaltic andesite samples from the western Basin and Range province using newly developed analytical procedures (Fig. 3). The ages are evaluated in terms of their reproducibility and consistency with $^{40}Ar/^{39}Ar$ whole-rock ages (Fig. 4). All ages were calculated based on at least seven individual aliquot analyses and show internally consistent data. The reproducibility appears to scale with parent nuclide concentration, with more radiogenic (>250 ppb U) and less radiogenic (100–200 ppb U) samples having reproducibility better than 4% and 11%, respectively. Samples 12-4-01A, VH-38-02, and 1003-CF-02 yield weighted-mean magnetite (U–Th)/He ages that are in good agreement with independent $^{40}Ar/^{39}Ar$ age constraints, demonstrating that magnetite (U–Th)/He ages provide accurate eruption ages. Only one sample (12-7-01C) exhibits a significant discrepancy between the two geochronometric systems. Additional $^{40}Ar/^{39}Ar$ and (U–Th)/He work on this and other samples from the same unit is required to resolve whether this discrepancy is geological or analytical in nature.

It is worthwhile noting that (U–Th)/He ages faithfully record eruption ages only if the sample has not been reheated to temperatures sufficiently high (>250 °C) for significant durations to partially or completely reset the age. The fact that $^{40}Ar/^{39}Ar$ and (U–Th)/He results for most samples in this study record the same age suggests that basaltic andesite samples did not experience significant reheating after eruption due to emplacement of subsequent flows.

4.3. Assumptions and important considerations

U and Th concentrations of magnetite dated in this study are approximately an order of magnitude lower than typical U and Th concentrations in intermediate to felsic volcanic rocks. (U–Th)/He dating of mineral phases with lower parent nuclide concentrations than the bulk rock or matrix is somewhat unusual and introduces additional complexities. While (U–Th)/He dating of apatite requires a morphometric correction for alpha-particle ejection (Farley et al., 1996), magnetite is likely to be subjected to alpha-particle implantation from surrounding matrix and neighboring minerals with higher parent nuclide concentrations. SEM back-scattered electron imaging in this study also point to the potential effect of He implantation from neighboring U- and Th-bearing minerals (Fig. 1B). Mechanical removal of the implantation-affected outer rind of magnetite by air abrasion is absolutely essential to this technique to correct for α-implantation and obtain reliable magnetite (U–Th)/He ages. Fig. 5 shows that these new (U–Th)/He ages are reproducible and independent of the effective U concentration (U + 0.23Th). This supports the notion that He ingrowth in the different magnetite samples is radiogenic in origin and is produced by the decay of U and Th, indicating that any effect of potential alpha implantation has been removed by mechanical air abrasion.

All (U–Th)/He age calculations in this study assume U-series secular equilibrium. U-series equilibrium might not be a valid assumption for magnetite (U–Th)/He dating of very young volcanic rocks (<1 Ma). In future studies of Quaternary volcanic rocks, accurate (U–Th)/He magnetite age calculations will need to consider fractionation of ^{230}Th ($t_{1/2}$ = 75 kyr) from ^{238}U and its effects on initial $^{230}Th/^{238}U$ disequilibrium (Farley et al., 2002; Schmitt et al., 2006).

One major limitation to improving the precision of magnetite (U–Th)/He geochronology is the ability to

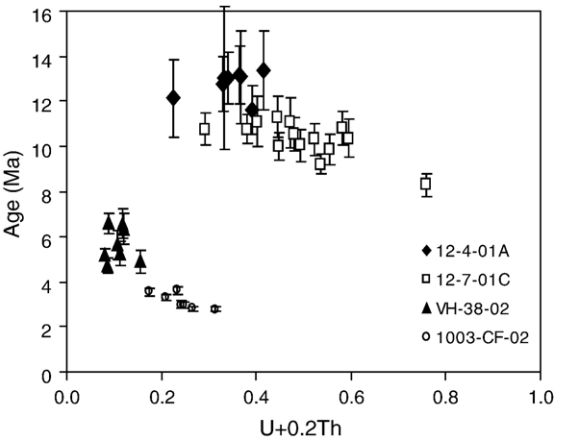

Fig. 5. Plot of magnetite (U–Th)/He age data against effective U concentration ([U] + 0.23[Th]). The lack of systematic aliquot age variation as a function of effective U concentration indicates that the He ingrowth in these magnetite samples and thus the (U–Th)/He age is not affected by He implantation from U and Th rich neighbouring crystals or inclusions and the air abrasion effectively removes alpha-implantation rind.

measure sub-ppm parent nuclide concentrations. The precision should be able to be improved significantly by measuring U, Th and Sm by Isotope Dilution Thermal Ionization Mass Spectrometry (ID-TIMS). Taking full advantage of the increased sensitivity this technique has to offer will allow us to decrease the number of grains analyzed in each aliquot while at the same time increasing the number of aliquots that can be analyzed.

5. Conclusions

In the magnetite (U–Th)/He dating case study presented here four basaltic to andesitic volcanic rocks from the Western U.S. were dated by both magnetite (U–Th)/He and whole-rock $^{40}Ar/^{39}Ar$ methods . The overall agreement between $^{40}Ar/^{39}Ar$ ages and the internally reproducible magnetite (U–Th)/He ages certainly suggests that magnetite (U–Th)/He dating holds great promise as an alternative volcanic geochronometer. The reproducibility of magnetite (U–Th)/He ages appears to be comparable to other commonly used (U–Th)/He thermochronometers, such as apatite or zircon(House et al., 2000; Reiners et al., 2002). The capability to date a mineral common to both intermediate and mafic rocks will expand (U–Th)/He applications beyond apatite- and zircon-bearing felsic volcanic rocks. More importantly, this geochronometer yields reliable eruption ages for volcanic rocks with complex to uninterpretable $^{40}Ar/^{39}Ar$ results. There are basaltic to intermediate volcanic rocks that are essentially undatable by traditional $^{40}Ar/^{39}Ar$ methods due to the presence of significant amounts of excess ^{40}Ar, recoil ^{39}Ar, and the lack and/or alteration of K-bearing phases. Despite these problems, geochronologic constraints on mafic to intermediate eruptions play a key role in several earth-science studies including paleomagnetic, tectonic/structural and chronostratigraphic studies. In these cases, magnetite (U–Th)/He dating may be a suitable and reliable alternative technique to whole-rock $^{40}Ar/^{39}Ar$ geochronology.

Acknowledgements

Funding for this project was in part provided by NSF grants EAR-0439824 (to Stockli and Walker) and EAR-0414817 (to Stockli). We are grateful to Richard Carlson for his editorial support as well as detailed and constructive reviews from Peter Reiners and an anonymous reviewer. We would also like to thank Matt Heizler and Kip Hodges for the $^{40}Ar/^{39}Ar$ data and Bob Goldstein for providing the magnetite sample from Bala, Kansas.

Appendix A. Supplementary data

Supplementary data associated with this article can be found, in the online version, at doi:10.1016/j.epsl.2007.04.044.

References

Aciego, S., Kennedy, B.M., DePaolo, D.J., Christensen, J.N., Hutcheon, I., 2003. (U–Th)/He age of phenocrystic garnet from the 79 AD eruption of Mt. Vesuvius. Earth Planet. Sci. Lett. 216, 209–219.

Baker, J., Waight, T., Ulfbeck, D., 2002. Rapid and highly reproducible analysis of rare earth elements by multiple collector inductively coupled plasma mass spectrometry. Geochim. Cosmochim. Acta 66, 3635–3646.

Blackburn, T.J., Stockli, D.F., Carlson, R.W., Berendsen, P., Walker, J.D., Winters, N.D., 2005. New (U–Th)/He age constraints on the emplacement of kimberlite pipes in north-eastern Kansas. Geochim. Cosmochim. Acta 69, 859.

Blondes, M.S., Reiners, P.W., Edwards, B.R., 2007. A. Biscontini, Dating young basalt eruptions by (U–Th)/He on xenolithic zircons. Geology 35, 17–20.

Boyce, J.W., Hodges, K.V., 2005. U and Th zoning in Cerro de Mercado (Durango, Mexico) fluorapatite: Insights regarding the impact of recoil redistribution of radiogenic 4He on (U–Th)/He thermochronology. Chem. Geol. 219, 261–274.

Bradley, D.B., 2004. Kinematic history of the Coaldale fault. Central Walker Lane Belt, University of Kansas.

Dodson, M.H., 1972. Closure temperature in cooling geochronological and petrological systems. Contrib. Mineral. Petrol. 40, 259–274.

Farley, K.A., 2002. (U–Th)/He dating: Techniques, calibrations, and applications. In: P.D., Ballentine, C.J., Wieler, R. (Eds.), Noble Gases in Geochemistry and Cosmochemistry. Reviews of Mineralogy, vol. 47, pp. 819–844.

Farley, K.A., Wolf, R.A., Silver, L.T., 1996. The effects of long alpha-stopping distances on (U–Th)/He ages. Geochim. Cosmochim. Acta 60, 4223–4229.

Farley, K.A., Reiners, P.W., Nenow, V., 1999. An apparatus for high-precision helium diffusion measurements from minerals. Anal. Chem. 71, 2059–2061.

Farley, K.A., Kohn, B.P., Pillans, B., 2002. The effects of secular disequilibrium on (U–Th)/He systematics and dating of quaternary volcanic zircon and apatite. Earth Planet. Sci. Lett. 201, 117–125.

Fechtig, H., Kalbitzer, S., 1966. The diffusion of argon in potassium bearing solids. In: Schaeffer, O.A., Zahringer, J. (Eds.), Potassium–Argon Dating. Springer, Heidelberg, pp. 68–106.

Fleck, R.J., Sutter, J.F., Elliot, D.H., 1977. Interpretation of discordant 40Ar/39Ar age spectra of Mesozoic tholeiites from Antarctica. Geochim. Cosmochim. Acta 41, 15–32.

Haggerty, S.E., 1991. Oxide Textures– A Mini-Atlas. In: Lindsley, D.H. (Ed.), Oxide Minerals: Petrologic and Magnetic Significance, vol. 25. Mineralogical Society of America, pp. 129–137.

Heizler, M., Sanders, R., 2005. 40Ar/39Ar Geochronology Results for Samples from Basalt. Geochronological Research Laboratory, New Mexico, NV.

House, M., Farley, K.A., Stockli, D., 2000. Helium chronometry of apatite and titanite using Nd-YAG laser heating. Earth Planet. Sci. Lett. 183, 365–368.

Krogh, T.E., 1982. Improved accuracy of U–Pb zircon ages by the creation of more concordant systems using an air abrasion technique. Geochim. Cosmochim. Acta 46, 637–649.

Ludwig, K.R., 2004. Isoplot/Ex rev 3.06 A Geochronological Toolkit for Microsoft Excel. Berkeley Geochronology Center.

Meesters, A.G.C.A., Dunai, T.J., 2002. Solving the production–diffusion equation for finite diffusion domains of various shapes Part II. Application to cases with alpha-ejection and nonhomogeneous distribution of the source. Chem. Geol. 186, 347–363.

Min, K., Reiners, P.W., Wolff, J.A., Mundil, R., Winters, R.L., 2006. (U–Th)/He dating of volcanic phenocrysts with high-U–Th inclusions, Jemez Volcanic Field, New Mexico. Chem. Geol. 227, 223–235.

Reiners, P.W., Farley, K.A., 1999. Helium diffusion and (U–Th)/He thermochronometry of titanite. Geochim. Cosmochim. Acta 63, 3845–3859.

Reiners, P.W., Farley, K.A., Hickes, H.J., 2002. He diffusion and (U–Th)/He thermochronometry of zircon: initial results from Fish Canyon Tuff and Gold Butte, Nevada. Tectonophysics 349, 247–308.

Schmitt, A.K., Stockli, D.F., Hausback, B.P., 2006. Eruption and magma crystallization ages of las Tres Virgenes (Baja California) constrained by combined 230Th/238U and (U–Th)/He dating of zircon. J. Volcanol. Geotherm. Res. 158, 281–295.

Spencer, A.S., Kohn, B.P., Gleadow, A.J.W., Norman, M., Belton, D.X., Carter, T.J., 2004. The importance of residing in a good neighbourhood: rechecking the rules of the game for apatite (U–Th)/He thermochronology. 10th International Fission Track Dating Conference, Amsterdam, p. 40.

Stockli, D.F., Tincher, C.R., Blackburn, T.J., Bradley, D.B., 2005. (U–Th)/He geochronometry of phenocrystic and xenocrystic silicate and oxide phases from volcanic rocks. Abstr. Programs - Geol. Soc. Am. 37, 198.

Tagami, T., Farley, K.A., Stockli, D.F., 2003. (U–Th)/He geochronology of zircon using Nd-YAG laser heating. Earth Planet. Sci. Lett. 207, 57–67.

Tincher, C.R., Stockli, D.F., 2004. Timing constraints on Cenozoic Faulting based on new Geochronological data in Eastern Queen Valley, Nevada. Abstr. Programs - Geol. Soc. Am. 36, 23.

Tsuyoshi, I., Sugimoto, K., Nagaishi, K., 2003. Determination of rare-earth elements in rock samples by an improved high-performance ion chromatography. Geochem. J. 37, 671–680.

Verchovsky, A.B., Begemann, F., 1993. Implanted radiogenic and other noble gases in crustal diamonds from northern Kazakhstan. Earth Planet. Sci. Lett. 120.

Ziegler, J.F., 1977. Helium: Stopping Powers and Ranges in all Elemental Matter. Pergamon.